

Dynamic flood topographies in the Terai region of Nepal

E.H. Dingle,^{1,2*}  M.J. Creed,² H.D. Sinclair,² D. Gautam,³ N. Gourmelen,² A.G.L. Borthwick⁴  and M. Attal²

¹ Department of Geography, Simon Fraser University, Burnaby, BC Canada

² School of GeoSciences, University of Edinburgh, Drummond Street, Edinburgh EH8 9XP, UK

³ Practical Action Consulting, Kathmandu 15135, Nepal

⁴ School of Engineering, University of Edinburgh, King's Buildings, Edinburgh EH9 3FB, UK

Received 19 November 2019; Revised 19 June 2020; Accepted 11 July 2020

*Correspondence to: E. H. Dingle, Department of Geography, Simon Fraser University, Burnaby, BC V5A 1S6, Canada. E-mail: elizabeth_dingle@sfu.ca

This is an open access article under the terms of the Creative Commons Attribution License, which permits use, distribution and reproduction in any medium, provided the original work is properly cited.

ESPL

Earth Surface Processes and Landforms

ABSTRACT: Flood hazard maps used to inform and build resilience in remote communities in the Terai region of southern Nepal are based on outdated and static digital elevation models (DEMs), which do not reflect dynamic river configuration or hydrology. Episodic changes in river course, sediment dynamics, and the distribution of flow down large bifurcation nodes can modify the extent of flooding in this region, but these processes are rarely considered in flood hazard assessment. Here, we develop a 2D hydrodynamic flood model of the Karnali River in the Terai region of west Nepal. A number of scenarios are tested examining different DEMs, variable bed elevations to simulate bed aggradation and incision, and updating bed elevations at a large bifurcation node to reflect field observations. By changing the age of the DEM used in the model, a 9.5% increase in inundation extent was observed for a 20-year flood discharge. Reducing horizontal DEM resolution alone resulted in a <1% change. Uniformly varying the bed elevation led to a 36% change in inundation extent. Finally, changes in bed elevation at the main bifurcation to reflect observed conditions resulted in the diversion of the majority of flow into the west branch, consistent with measured discharge ratios between the two branches, and a 32% change in inundation extent. Although the total flood inundation area was reduced (−4%), there was increased inundation along the west bank. Our results suggest that regular field measurements of bed elevation and updated DEMs following large sediment-generating events, and at topographically sensitive areas such as large river bifurcations, could help improve model inputs in future flood prediction models. This is particularly important following flood events carrying large sediment loads out of mountainous regions that could promote bed aggradation and channel switching across densely populated alluvial river systems and floodplains further downstream. © 2020 The Authors. *Earth Surface Processes and Landforms* published by John Wiley & Sons Ltd

KEYWORDS: Nepal; flood inundation; channel mobility; bifurcation; Delft3D

Introduction

Rivers sourced from the Himalayan mountains irrigate the Indo-Gangetic Plain and support about 10% of the global population. Many of these rivers are also the source of devastating floods, with effects further compounded where isolated communities, living on the river floodplain, lack disaster risk management and resilience measures. In Nepal alone, flood disasters were responsible for over US\$130 million losses and nearly one-third of all natural disaster-related deaths between 2001 and 2008 (Risk Nexus, 2015). Specific examples include the 2008 Kosi River avulsion (e.g. Sinha, 2009; Chakraborty *et al.*, 2010), and the 2013 Uttarakhand floods that killed over 5000 people and are viewed as India's worst natural disaster since 2004 (e.g. Rana *et al.*, 2013). While early warning systems saved many lives in the 2014 Karnali River floods, which impacted 120000 people living in the Terai region in western Nepal, gaps in the disaster management system were still

apparent. Water levels rose to around 16 m at Chisapani (where the river exits the mountain front and enters the Indo-Gangetic Plain), 1 m higher than the previous record in 1983; the return interval for this 2014 event was estimated to be 1000 years (Risk Nexus, 2015). In the post-event review capability report produced in the aftermath of the flood (Risk Nexus, 2015), stakeholders highlighted that flood risk is currently underestimated, a potential cause being that changes to the channel bed are not included in flood risk assessments. Where sediment deposition within channels reduces channel capacity, specific event discharges (e.g. the 20-year flood discharge of $\sim 17000 \text{ m}^3 \text{ s}^{-1}$) are likely to increase inundation extent because channel capacity will be exceeded earlier in the rising limb of the flood hydrograph, and remain over bank for longer (Stover and Montgomery, 2001; Lane *et al.*, 2007; Slater *et al.*, 2015). Flood hazard may also be incorrectly estimated in other similar major river systems downstream of the Himalayan mountains across the Indo-Gangetic Plain, many of which are largely

aggradational in nature, with high rates of channel avulsion (e.g. Sinha, 2009). Given this context, we use the term 'dynamic flood topographies' in this setting to emphasize the constant change and dynamic interaction of mobile alluvial landscapes with flood waters.

Changes in river course and sediment dynamics that alter the morphology (e.g. channel geometry and form) of river channels and adjacent floodplain have been shown to modify the likelihood of flooding (e.g. Stover and Montgomery, 2001; Lane *et al.*, 2007; Slater *et al.*, 2015, 2019), yet these processes are rarely considered in flood hazard assessment. Flood inundation extent is primarily determined by flow discharge, in particular the magnitude of peak flow. But, for a given flow, the extent to which water levels overtop the local bank and flow out onto the adjacent floodplain is also controlled by channel conveyance (Lane *et al.*, 2007). River systems downstream of the Himalayan mountain front are typically described as shallow, aggrading alluvial systems (e.g. Sinha *et al.*, 2005; Tandon *et al.*, 2006; Dingle *et al.*, 2016), which are characterized by large sediment loads (Sinha and Friend, 1994; Lupker *et al.*, 2012) and high rates of lateral channel migration and avulsion (Chakraborty *et al.*, 2010; Dingle *et al.*, 2020). Sediment accumulation in channels may be caused by simple natural variability in sediment flux from upstream parts of the catchment, but also by changes in land use, engineering works (e.g. damming), climate change (e.g. increased rainfall intensity), and landslides (e.g. resulting from intense monsoon and/or earthquake). This can result in alluvial channels with fluctuating bed elevations (and therefore channel conveyance)

if sediment is not immediately evacuated, which may modify flood inundation extent during subsequent high flow discharges. Understanding both hydrological processes and sediment dynamics is key to mitigating flood risk in aggrading, low-relief landscapes characterized by rivers with high sediment supply (e.g. Aalto *et al.*, 2003). Flood hazard maps used to inform communities downstream of the Himalayan mountains and build resilience to these types of events are based on static and outdated digital elevation models (DEMs), which do not reflect the dynamic river configuration or hydrology (Risk Nexus, 2015).

Here, we use a new Delft3D flood inundation model that incorporates field geomorphological evidence (e.g. measured channel geometry and bed elevations) and a high-resolution DEM of the landscape that more closely reflects the current configuration of the Karnali River in west Nepal (Figure 1). The first aim of this paper is to examine the change in flood inundation extent resulting from a change in model and DEM. The new 2D hydrodynamic model is tested for several flood scenarios and the results compared against existing modelled predictions generated using a different hydrological model (1D HEC-RAS, undertaken by the Nepal Department of Hydrology and Meteorology – DHM). The effect of changing the DEM is examined in terms of improved spatial resolution and the difference in channel configuration between the two DEMs (that were captured more than 10 years apart). The second aim is to test how modelled flood inundation extent responds to varying channel bed elevation, to simulate bed aggradation and incision that might be expected following

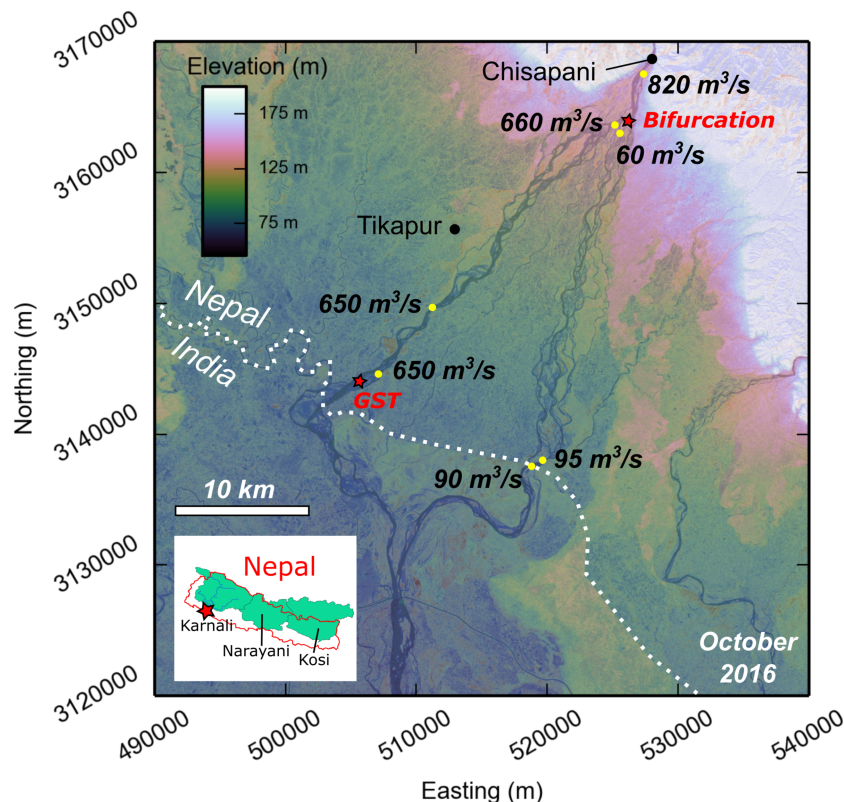


FIGURE 1. Karnali River downstream of Chisapani. The positions of the bifurcation and gravel–sand transition (GST) are shown by red stars. Average discharge measurements from ADCP surveys on the Karnali River in October 2016 are also shown (yellow circles). Of the $\sim 820\text{ m}^3\text{ s}^{-1}$ recorded at Chisapani, $\sim 80\text{--}90\%$ of flow is directed into the west branch of the river at the bifurcation. ADCP surveys at the bifurcation point did not capture the entirety of flow directed into the east branch, as there was an additional channel further east which was not accessible. Based on the discharge measurements made on the east branch further downstream ($90\text{--}95\text{ m}^3\text{ s}^{-1}$), this small channel was likely to only be conveying $\sim 30\text{ m}^3\text{ s}^{-1}$. The $\sim 100\text{ m}^3\text{ s}^{-1}$ lost between the upstream sample ($820\text{ m}^3\text{ s}^{-1}$) and the bifurcation point may also be due to water diversion into the canal network immediately downstream of the Chisapani bridge, to flow into small braid channels in the floodplain, and to underground flow through the thick porous sediment (which is absent at the most upstream site where the channel is bedrock). Data sources: 30m SRTM DEM (coordinates in UTM Zone 43 N) and Sentinel-2 optical satellite imagery (captured 26 October 2016). [Colour figure can be viewed at wileyonlinelibrary.com]

delivery of sediment pulses into the foreland basin. The final aim of the paper is to assess the sensitivity of flow routing and flood inundation extent, downstream of a major bifurcation node, to changes in bed elevation. We do this through updating bed elevations at a large bifurcation node on the Karnali River to reflect field observations, and compare the modelled results to observed discharge ratios between the two branches. The results demonstrate the sensitivity of model predictions of fluvial inundation to the horizontal and vertical resolution of the DEM. This is particularly relevant in the low-gradient setting of the Terai. Additionally, we show that changes in bed elevation, typical of changes induced by increased sediment supply from the mountain catchment, drive flood inundation into areas that were previously unaffected.

Methods

Geomorphological setting

The Karnali basin has a drainage area of $\sim 43\,000\text{ km}^2$ upstream of the mountain outlet at the town of Chisapani (Figure 1), where the channel exits a confined bedrock gorge and flows out onto the alluvial Indo-Gangetic Plain. In the upper reaches of the alluvial plain, the channel is characterized by a coarse gravel to cobble bed which fines downstream ($D_{50} = 46\text{--}148$ mm between the mountain front and gravel–sand transition; Quick *et al.*, 2019). The gravel channel is braided with exposed gravel bars (at low flow) and mature, vegetated islands. At ~ 5 km downstream, the channel bifurcates into two branches. The gradient of the gravel reaches, which extend to the gravel–sand transition at ~ 40 km downstream in each branch, is $0.001\text{--}0.002\text{ mm}^{-1}$ (Dingle *et al.*, 2020). The gravel–sand transition occurs over a distance of $\sim 2\text{--}3$ km, downstream of which the channel bed is exclusively sand, and the two branches of the Karnali River rejoin. The channels are considerably more mobile in the sand-bed portion of the river system and can migrate hundreds of metres in a single year (Dingle *et al.*, 2020). The average gradient of the sand channel is approximately half that of the gravel reach.

The flow is seasonal, and dominated by the Indian Summer Monsoon. Since 1962, when the gauging station at Chisapani was installed, the average daily discharge recorded from November to April ranges from 400 to $600\text{ m}^3\text{ s}^{-1}$, but can be as low as $200\text{ m}^3\text{ s}^{-1}$. The peak monsoon flood has been observed as early as June and as late as October, and peak flood usually arrives in August. From the gauging station records, peak flood discharges exceed $5000\text{ m}^3\text{ s}^{-1}$ annually. The maximum instantaneous discharge since 1962 was recorded on 15 August 2014, estimated as $\sim 22\,000\text{ m}^3\text{ s}^{-1}$.

Digital elevation model

TanDEM-X imagery was used to generate DEMs of the channel system. TerraSAR-X has a repeat period of 11 days, and data acquired by both satellites, flying in tandem, have a spatial resolution on the order of 1 m (Krieger *et al.*, 2007; Eineder *et al.*, 2011), thereby providing excellent temporal and spatial resolution for observing topography and how it changes. The radar platforms enabled us to use imagery acquired in non-daylight hours and cloudy conditions, in contrast to optical platforms. We derived a 10m-resolution DEM dated 23 February 2013 from conventional SAR interferometric processing of bi-static TanDEM-X imagery (Dehecq *et al.*, 2016). A Shuttle Radar Topography Mission (SRTM) DEM was used as

reference during the unwrapping stage to minimize unwrapping errors.

No-data values in the 2013 TanDEM-X DEM (10m spatial resolution) were filled with data from a 30m-resolution SRTM DEM (captured in 2000). In general, no-data regions corresponded with the wet portion of the river channel. In the regions that were too large to interpolate elevations between opposite banks, pixels in the 30m SRTM DEM were resampled to the same resolution as the TanDEM-X DEM (10m) prior to filling. Topographic noise was then suppressed across the entire DEM using a Wiener filter (Pelletier, 2013; Grieve *et al.*, 2016). The large vertical error associated with the SRTM data used to patch the no-data values in the TanDEM-X data resulted in large artificial jumps in the elevation of the channel bed (10–20m changes in elevation between adjacent pixels), despite the Wiener filtering. This may in part be due to the shift in channel position between the times that the two DEMs were captured. In order to correct for this, the region of the DEM which corresponded to the active channel was smoothed using a focal mean smoothing radius of 3×3 pixels. This was repeated until the area of the DEM representing the active channel was effectively free of artificial highs and lows. Given the exceptionally low gradient and relief of the Karnali channel and its adjacent floodplain, this method generated a reasonable representation of topographic conditions across the study area.

The vertical error or root-mean-square error (RMSE) associated with the SRTM DEM elevations can vary between ± 6.2 and ± 22.35 m, depending on vegetation cover (Carabajal and Harding, 2006; Rodriguez *et al.*, 2006; Wendi *et al.*, 2016). The RMSE of the TanDEM-X DEM is ± 1.1 to ± 1.8 m (Wessel *et al.*, 2018).

Field measurements and data collection

Measurements of channel bed elevation and floodplain (bank top) elevation were made in October 2016 using an RTK-GPS system, resolving to centimetre vertical accuracy. For land surface elevations, a number of RTK-GPS surveys were carried out, while absolute channel bed elevations were measured using the same GPS system mounted to a Sontek R9 Acoustic Doppler Current Profiler (ADCP) (Figure 2). Channel transects were surveyed at seven locations using the ADCP to estimate water discharge at Chisapani (upstream of the bifurcation) and at locations down the west and east branches to ascertain the proportion of flow diverted down each branch (Figure 1). The bank surveys provided information on bankfull channel depth when combined with ADCP data. The elevations of the channel bed down each branch at the bifurcation were surveyed in particular detail because the bed elevations at this location control the ratio of flow diverted down each branch in the Delft3D model.

Model setup

Delft3D was used to create a 2D depth-averaged hydrodynamic model of the Karnali river system, where vertical accelerations were neglected and hydrostatic pressure assumed. The model domain was defined on an orthogonal, curvilinear, structured mesh, with 56744 grid cells (Figure 3). The number of cells was chosen to ensure grid convergence in the most important areas of the domain for the study, including the main river channel and sensitive, flood-prone regions. Grid cell length ranged from 15 to 50m inside the river, and increased up to 1000m at the east and west domain boundaries, where no flow was expected, even in extreme flood events. The grid

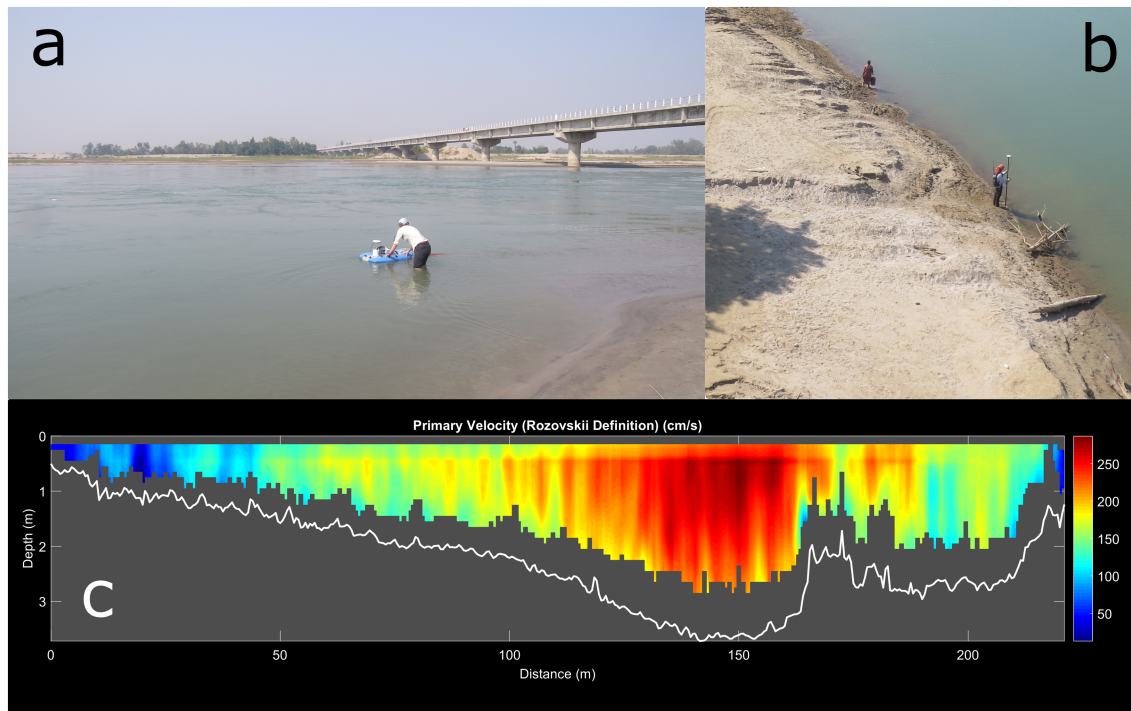


FIGURE 2. Field surveys carried out on the Karnali River in October 2016. (a) Channel geometry and discharge were measured using an ADCP at locations shown in Figure 1. (b) Absolute bank elevations were determined using an RTK-GPS system to complement the ADCP surveys. (c) Example of the ADCP data output using VMT v4.09 (Parsons *et al.*, 2013) showing cross-section channel geometry and primary flow velocity cm s^{-1} in the downstream direction. [Colour figure can be viewed at wileyonlinelibrary.com]

aspect ratio, which determines the smoothness of the flow in the model from cell to cell, ranged from 1.4 to 2.2 within the river and flood-sensitive areas, and up to 2.5 at the outer domain grid cells. For the purpose of the present study, which investigates the effect that DEM age and resolution have on flood inundation maps, sediment transport was not included in the numerical model.

The boundaries of the east and west river channels were obtained from the 30m SRTM DEM. The grid was generated inside the main channels, and then expanded out to the east

and west domain boundaries. The downstream boundary is defined where the two branches of the river reconnect, on the Indian side of the Nepal–India border (Figure 1). The upstream boundary is located at the river gauging station in the town of Chisapani, where discharge measurements are recorded regularly.

A time-series hydrograph of the discharge was specified at the upstream boundary, located at the Chisapani gauging station, where daily measurements, between 1962 and 2010, were obtained from the Nepal DHM records. In the absence

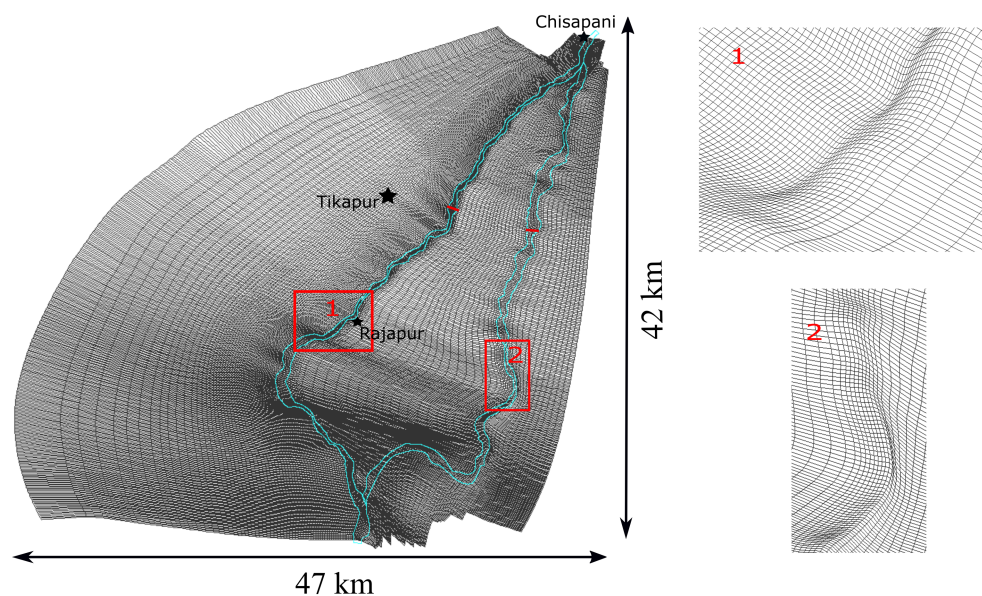


FIGURE 3. 2D depth-averaged model dimensions and structured mesh (Delft3D software). The mesh was generated inside the main river channels (boundaries shown in blue) and expanded outwards to the east and west domain boundaries. River cross-section locations for evaluating discharge down the east and west branches are shown by red lines. Selections (1) and (2) show a sample of the higher-resolution mesh within the main river channel of the west and east branches, respectively. The largest municipalities – Tikapur, Rajapur, and Chisapani – are represented by black stars. [Colour figure can be viewed at wileyonlinelibrary.com]

of discharge or water level data at the downstream boundary, a transmissive boundary condition was specified at the outlet of the domain. The transmissive condition defines the gradient of the water surface, estimated as the gradient of the bathymetry, 0.0001 in this case.

The river channel was filled with water initially, with the same water depth assigned everywhere in the river. Average daily discharge measurements recorded at Chisapani gauging station were used as the input discharge for the model. The 20-year flood, an event that has a 1 in 20 chance of exceedance each year, was modelled in all of the scenarios considered. The discharge of the 20-year flood is $\sim 17000\text{m}^3\text{ s}^{-1}$, estimated by fitting the maximum annual instantaneous discharge measurements from 1962 to 2014 to a Gumbel distribution (see supplementary data file). A flood of this magnitude was recorded at Chisapani in June 2013. Daily discharge measurements from February to June 2013 (hydrograph available in supplementary material) were used as model input, allowing sufficient time for the model to reach equilibrium prior to the peak flood.

To investigate how the DEM resolution and the type of model used can affect model output, the 20-year flood model was run using TanDEM-X and 30m SRTM elevation data. The outputs of the 20-year flood model were compared between: (1) an existing 1D HEC-RAS model (obtained from the DHM) using

the SRTM DEM as the base topographic data (Figure 4a); (2) the Delft3D model using the same SRTM DEM base data (Figure 4b); (3) the Delft3D model using the new 10m TanDEM-X data as base topographic data (Figure 4c; Table 1); and (4) the Delft3D model using the TanDEM-X data resampled to 30m, as base topographic data (Figure 4d). In these instances, the river bed elevation was taken from the DEM directly. It is assumed that model configurations and subsequent scenarios run using unmodified DEMs do not account for channel bathymetry, and instead the elevation within the channel boundary is effectively the elevation of the water surface.

Using the results from the Delft3D model with unmodified 10m TanDEM-X data as a baseline scenario (Scenario 1), the following scenarios were investigated using the Delft3D model and the same hydrological inputs (20-year flood discharge).

Scenario 1 (baseline)

River bed elevation obtained from the TanDEM-X DEM directly, where the channel elevation represents the water surface.

Scenario 2 (uniformly lowered bed)

Sampled flow depths surveyed in October 2016 at a number of locations (e.g. Figures 1 and 2) were on average 1.5–2m. The

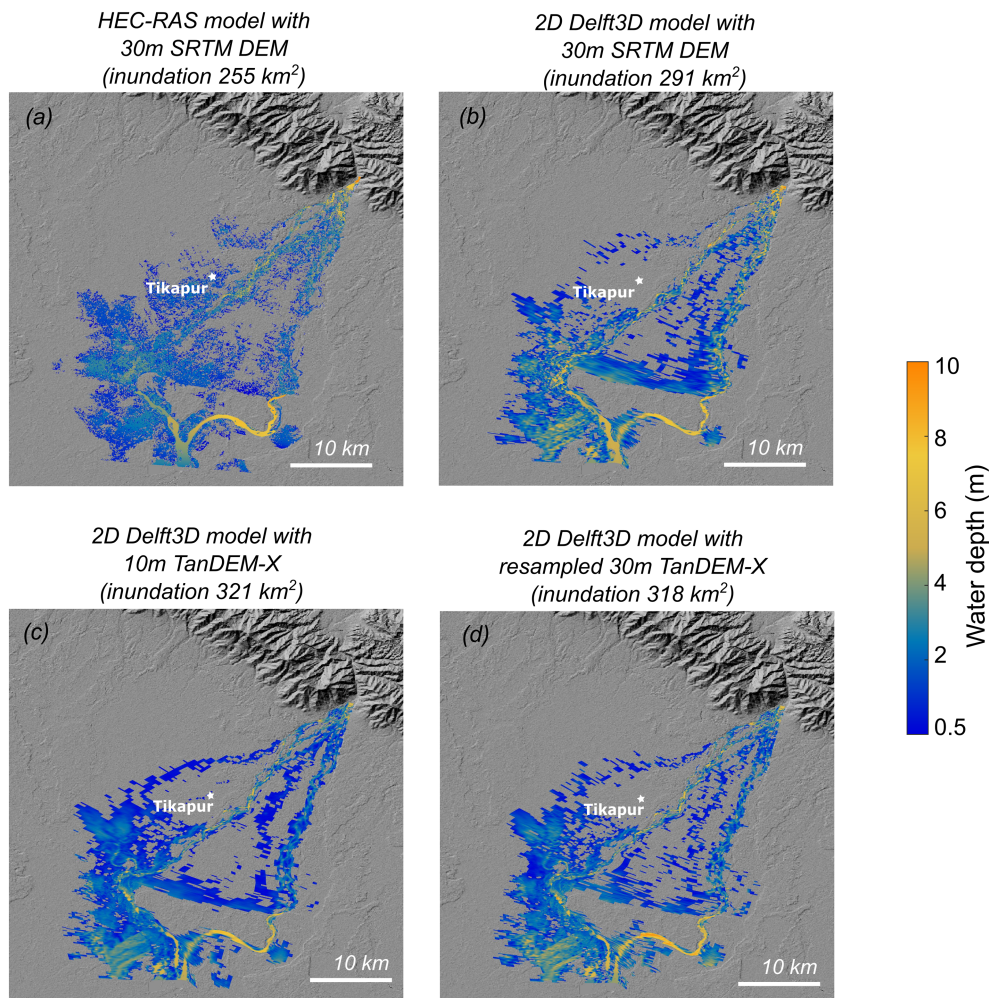


FIGURE 4. Inundation extent and water depth ($>0.5\text{m}$) for a 1 in 20-year flood discharge for (a) the existing HEC-RAS hydrodynamic model and SRTM DEM (inundated area 265km^2), (b) using the new Delft3D model and SRTM DEM (inundated area 291km^2), (c) for Scenario 1 using the Delft3D model and new 10m TanDEM-X DEM (inundated area 321km^2), and (d) for Scenario 1 using the Delft3D model and 30m resampled TanDEM-X DEM (inundated area 318km^2). The same model configurations are presented showing inundation depths $>0.05\text{m}$ in the supplementary material. [Colour figure can be viewed at wileyonlinelibrary.com]

Table 1. Percentage change in the inundation extent between scenarios and model configurations (km²)

	Scenario 1 (unmodified TanDEM-X DEM)	Scenario 2 (uniformly lowered bed)	Scenario 3 (bifurcation modification)	Scenario 4 (resampled DEM)	SRTM DEM	SRTM DEM with 1D HEC-RAS model
% Change in area for inundation depths >0.5 m	Baseline (320 km ²)	−36%	−32%	−0.9%	−9.5%	−20.5%

surface of the DEM within the channel boundaries was uniformly lowered by 1.8 m across the main channel, approximating field observations.

Scenario 3 (bifurcation modification)

This scenario is an extension of Scenario 2. In October 2016, at the bifurcation, bed elevations measured from ADCP surveys were up to 5 m lower than the DEM values in the west branch and 0.5–1 m lower in the east branch. In this scenario, as in Scenario 2, the river bed elevation was first uniformly reduced by 1.8 m everywhere within the main river channel. The bed elevations at the bifurcation were then further adjusted to reflect the field observations recorded in October 2016. At the bifurcation, the west branch river bed was reduced further, by up to 3.2 m (to a total of up to 5 m depth), and 0.8–1.3 m was added back to the river bed elevations in the east branch (to generate a total channel depth of 0.5–1 m). Changes to the

DEM were made on a cell-by-cell basis over a downstream distance of 1–2 km to maintain the bed slope and avoid generating artificial discontinuities in the bed.

Results

Field measurements

ADCP transects surveyed in October 2016 revealed a large asymmetry in the distribution of flow between the two branches of the Karnali River downstream of the bifurcation. From the 820 m³ s^{−1} discharge measured at the exit of the bedrock canyon at Chisapani, ~80% of the flow was diverted into the west branch and only ~7% of flow was diverted into the east branch (Figure 1). The remaining ‘missing’ ~13% is likely due to a combination of: capture in smaller braid channels on the west

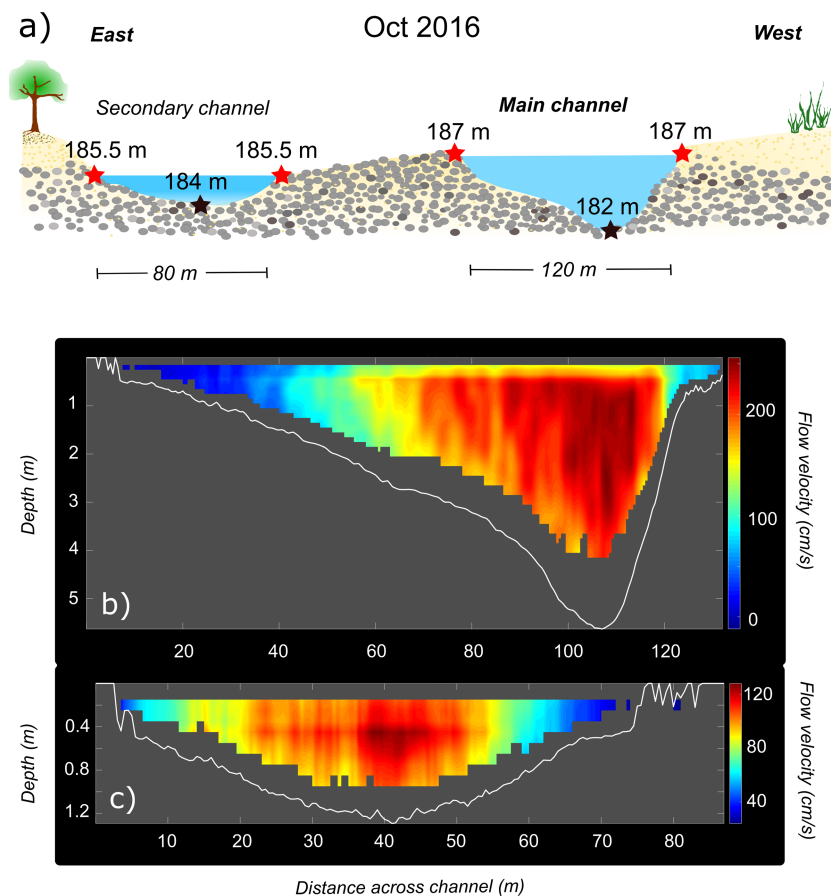


FIGURE 5. Karnali cross-sections downstream of bifurcation, looking downstream. (a) Schematic cross-section showing the difference in absolute bed and bank elevation between the west and east branches immediately downstream of the main bifurcation node, based on ADCP transects in October 2016 (shown in b and c). (b) ADCP transect from the main channel (west branch) showing channel depth and flow velocity. (c) ADCP transect from the secondary channel (east branch). Both ADCP transects have been processed using VMT v4.09 (Parsons *et al.*, 2013). [Colour figure can be viewed at wileyonlinelibrary.com]

and east branches (which were not surveyed due to access issues), diversion into a canal intake just downstream of the Chisapani transect, and underground flow through the porous alluvium. Transects taken on the west and east branches immediately downstream of the bifurcation revealed that the absolute bed elevation of the channel was ~ 2 m lower in the west (main) branch, and that flow at the time of the survey was ~ 3.5 m deeper in the west branch than the east (Figure 5).

Modelling results

The 1D HEC-RAS model using the SRTM DEM was developed by the Nepal DHM by extracting multiple topographic cross-sections at critical locations perpendicular to the Karnali river channel (personal communication, October 2019), including at the bridges and the bifurcation point (Figure 1), and interpolating the results between cross-sections. The difference in inundation extent between the 1D HEC-RAS model results and the 2D Delft3D model, visually represented in Figures 4a and b, is likely due to the spatial resolution and the selection of cross-section data in the HEC-RAS model. For example, generally, the west branch river channel is deeper in the Delft 3D model (Figure 4b) than the HEC-RAS model (Figure 4a), and less water is observed on the western floodplain, near Tikapur in the Delft3D model (see Figure 4). The 2D Delft3D model may represent the channel geometry more accurately, thus increasing the channel capacity and containing the flow in this location for the given discharge.

Changing the DEM resolution and age (from SRTM to TanDEM-X) within the Delft3D model resulted in a 9.5% increase in flood inundation extent for depths greater than 0.5 m (Figures 4b and c; Table 1). Visually, the smaller secondary channels or braid channels north of the town of Tikapur (Figure 4c) are better represented by the higher spatial resolution of the TanDEM-X data. The depth in the east branch of the river is larger in the SRTM DEM compared to the TanDEM-X DEM, suggesting a greater percentage of the flow is routed down the east branch. The east bank of the east branch is characterized by a 5–10 m-high alluvial terrace with dense tree cover provided by the Bardia National Park. Consequently, when more flow is diverted down the east branch in Figure 4b, the flood is contained by the higher bank elevation, reflected by higher water depth within the channel (i.e. yellow pixels). This causes slightly increased flooding in the central floodplain area, along the west bank of the east branch of the

river, and decreased flooding along the banks of the western branch. Resampling the TanDEM-X to a coarser-resolution 30 m DEM resulted in a 1% decrease in inundation area (Figure 4d). In Figure 4d, the distribution of flow down the two branches is similar to that for the 10 m TanDEM-X (Figure 4c), and the depth in the east branch is smaller for the 30 m TanDEM-X than for the 30 m SRTM (Figure 4b). Flood inundation maps for depths >0.05 m, included in the supplementary material, follow these trends.

When the bed elevation is reduced in Scenario 2, overall flooding extent is reduced by $\sim 36\%$ (Table 1), as seen by comparing Figures 6a and b. Lastly, when the bed elevation is reduced and the bifurcation bed levels are changed in Scenario 3 to integrate the bed levels observed in the field in October 2016 (Figure 6c), more flooding is observed than in Scenario 2 (-32% compared to -36% , Table 1), particularly in the west floodplain.

Reducing the bed elevation uniformly from Scenario 1 to 2 results in a 36% decrease in inundation area (Table 1), and a notable decrease in flood extent in the western floodplain (Figure 6b). When the bifurcation is then modified (Scenario 3, Figure 6c), slightly more flooding is observed in the western floodplain but the flood extent is reduced in the central floodplain that separates the two branches, when comparing to Scenario 2 (Figure 6b). In Scenario 2, the east branch is the major river branch conveying the majority of the flow (Figure 7b). Similarly to the SRTM DEM (Figure 4b), when more flow is diverted down the east branch in Figure 6b, the flood is contained by the higher bank elevation, reflected in the higher water depths within the channel. This results in slightly increased flooding on the banks of the eastern branch and decreased flooding along the banks of the western branch.

Figure 7 presents discharge hydrographs in the east and west branches for Scenarios 1, 2, and 3, for Delft3D models using the 10 m TanDEM-X data, for the 20-year flood discharge. When the DEM is unchanged, the flow is evenly distributed down the west and east branches, with slightly more flow (approximately 55–60%) in the west branch. When the bed elevation is uniformly reduced by 1.8 m (Figure 7b), the east branch becomes the main channel, accounting for between 75 and 90% of discharge before the peak flood arrives, and 60% at peak flood discharge. The biggest change in flow distribution is observed when the DEM is modified and the bed elevation at the bifurcation is updated to reflect the October 2016 field observations. In Figure 7c, approximately 85–90% of flow

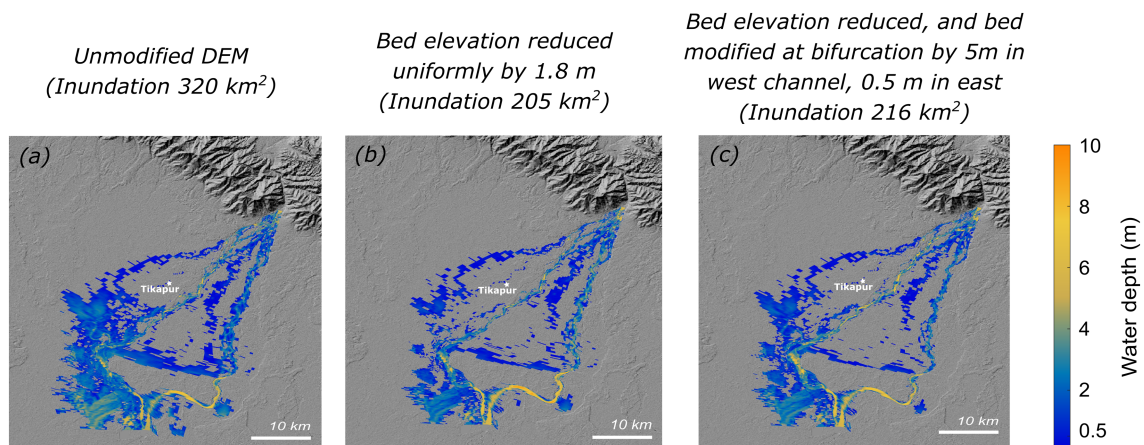


FIGURE 6. Inundation extent and depth (>0.5 m) for a 1 in 20-year flood discharge for (a) Scenario 1, DEM unmodified, bed elevation given by surface water level in the DEM; (b) Scenario 2, where bed elevation is reduced by 1.8 m; (c) Scenario 3, where bed elevation is reduced by 1.8 m, except at the bifurcation where the bed is reduced by 5 m in the west branch and 0.5 m in the east branch. [Colour figure can be viewed at wileyonlinelibrary.com]

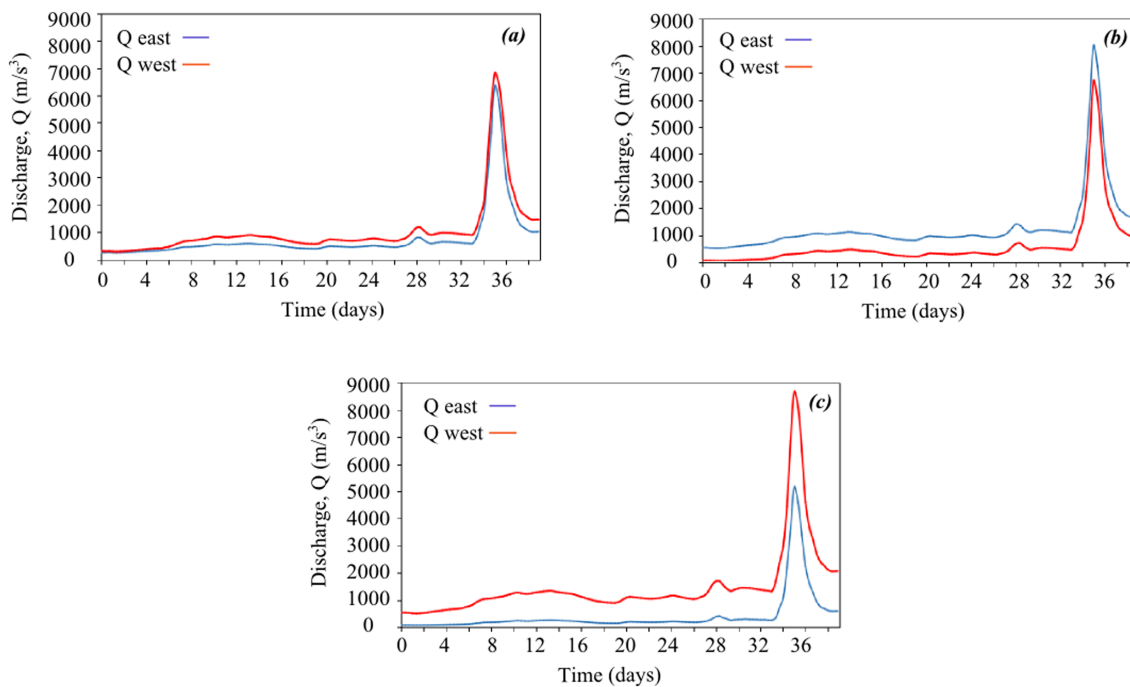


FIGURE 7. Modelled hydrographs for the 20-year flood, in the east and west branches for (a) Scenario 1 (baseline, no change to DEM), (b) Scenario 2 (uniformly lowered bed), and (c) Scenario 3 (uniformly lowered bed and bifurcation modified). [Colour figure can be viewed at wileyonlinelibrary.com]

goes down the west branch before the peak flood, and approximately 65% at peak flood flow. Before the peak flood arrives (beginning at ~34 days, Figure 7c), the discharge ratio is similar to the field observations from October 2016 (Figure 1).

Discussion

The reduction in flood inundation area between Scenario 1 (baseline scenario with channel depth defined by the surface water level in DEM) and Scenario 2 (uniformly lowered bed) is indicative of how flood inundation patterns may respond to episodes of extreme channel incision, such as might be expected following large storms. In the opposite scenario (i.e. where a channel evolves from Scenario 2 to Scenario 1), such as might be expected following periods of enhanced sediment delivery into the foreland basin (e.g. earthquake-induced landslide inputs), there may be several metres of bed aggradation, resulting in a large increase in inundation extent (e.g. Keefer, 1999; Chen and Petley, 2005). Scenario 3 used the bed elevations of Scenario 2, but modified river bed elevations at the bifurcation area to represent elevations observed in the field in October 2016. Changing bed elevations in this small region of the river increased downstream flood extent (–32% compared to –36%, Table 1), with new areas predicted to experience flow depths >0.5m (Figures 6b and c). As a result of the elevation changes at the bifurcation, the main or dominant river channel (with the greater discharge) switched from the east to the west between Scenario 2 and Scenario 3 (Figures 7b and c). The modelled hydrographs of Scenario 3, shown in Figure 7c, represent most accurately the discharge distribution observed in October 2016 (Figure 1).

The increase in inundation extent associated with the change in DEM (from SRTM to TanDEM-X in Figures 4b and c) may also relate to improved representation of the channel geometry and the braided channel network. In the coarser SRTM DEM, only channels or braids with widths greater than two pixels (>60 m) are likely to be captured in the DEM. With the higher-resolution TanDEM-X DEM, the channel network in

the upper portion of the system is better represented, especially where the flow geometry is characterized by much narrower (<60m) and multiple channel braids than the downstream portion. Improved representation of these smaller secondary channel networks allows flow to reach adjacent regions of the floodplain in the model more easily than the topographic conditions represented by the SRTM DEM. This results in an increase in the number of wet cells and hence inundation extent for the same flood discharge. The relatively small change (<1%) in inundation extent between the 10m TanDEM-X and resampled 30m TanDEM-X DEMs, in comparison to the change from the older 30m SRTM to the newer unmodified 2013 TanDEM-X DEM (9.5%), suggests that reduced vertical error and improved representation of the current channel configuration are likely to have greater impact on flood inundation modelling than simply improving the horizontal resolution of the DEM. In river systems as dynamic as the Karnali River, accurate representation of channel configuration and elevation is a prerequisite for improved flood inundation modelling.

Given the highly variable seasonal discharge and large sediment loads exported by rivers into the Ganga Plain (e.g. Tandon *et al.*, 2006), variable bed elevation and high channel migration rates are key geomorphological features of these systems which need to be incorporated into predictive flood hazard modelling. The results presented here demonstrate the sensitivity of modelled flood inundation extents to (1) sediment-driven changes in bed elevation and (2) the temporal variability in channel position based on two DEMs captured 12 years apart. Our results highlight the role that these processes play in modelled flood inundation extent, and that geomorphological processes need to be incorporated to improve future flood hazard prediction.

Limitations

A combination of large sediment loads, poorly consolidated and unvegetated channel banks, and peaked seasonal hydrographs contribute to the development of highly dynamic

and mobile river channels across low-relief landscapes, such as those downstream of the Himalayan mountains. Large storms or sediment-generating events (e.g. widespread earthquake-induced landsliding) also drive aggradation in the downstream alluvial system, which can decrease channel capacity (e.g. Goswami, 1985; Keefer, 1999; Chen and Petley, 2005; Lane *et al.*, 2007; Dingle *et al.*, 2017). In the modelling work presented here, a uniform reduction in bed elevation is assumed between two scenarios (from 1 to 2; Figure 6). Sediment deposition or erosion downstream of the mountain front is unlikely to occur in this spatial fashion. Intuitively, it would be expected that gravel (and coarser) grain sizes will be deposited upstream of the gravel–sand transition, which occurs ~40–45 km downstream of Chisapani (Figure 1). If the majority of sediment delivered out of the mountains is sand-sized or finer, this material is expected to remain largely in transport and be deposited on the floodplain (if there is significant overbank flow) or within the channel further downstream of the gravel–sand transition. Deposition of this sediment onto the channel bed is also likely to initiate enhanced lateral migration of sand-bedded channels (e.g. Dingle *et al.*, 2020), as channels can be highly unstable when transporting high sediment loads (e.g. Montgomery *et al.*, 1999). In contrast, rates of vertical incision are likely to be highest closest to the mountain front where channel gradients are greatest. In general, the thickness of sediment deposited or eroded within these types of channels is likely to change with distance downstream, in keeping with patterns of subsidence-driven accommodation across a foreland basin (e.g. Flemings and Jordan, 1989).

The changes in bed elevation used in the different scenarios modelled by Delft3D lie within the vertical error or RMSE associated with the SRTM DEM elevations, which vary between ± 6.2 and ± 22.35 m (Carabajal and Harding, 2006; Rodriguez *et al.*, 2006; Wendi *et al.*, 2016). This highlights the potential error in flood inundation extents modelled using low-resolution DEMs of low-relief landscapes where small changes or inaccuracies in river bed elevation can result in significantly under- or overestimated flood inundation extents. This is further compounded by outdated DEMs, such as the 30 m SRTM DEM (which was captured in 2000), given that mobile channels can migrate hundreds to thousands of metres across their floodplains in a single year (e.g. Coleman, 1969; Constantine *et al.*, 2014; Dingle *et al.*, 2019). The value of flood inundation models based on outdated topographic data in these types of morphologically active regions is questionable. In comparison, the RMSE of the TanDEM-X DEM is considerably lower at ± 1.1 to ± 1.8 m (Wessel *et al.*, 2018). When the 30 m SRTM data are used, the modelled inundation extent is reduced (Figure 4b), with 9.5% less inundation area than the TanDEM-X model. However, in certain areas of the western

floodplain, the depth of the flood is increased in the SRTM model. This could be exacerbated by the error in the SRTM data; overestimated elevations could inhibit the flow, and underestimated elevations could cause accumulation or ponding of flow. The difficulty in validating the numerical models lies in the lack of accurate flood information, which is presently only available in word-of-mouth form. The orbital interval of satellite imagery is typically several weeks, so is unlikely to capture maximum flood extents. The quality of images is also complicated by increased cloud cover during the monsoon season.

Topographically sensitive points in the channel network

Small changes in channel bed elevation at particularly sensitive points (such as major bifurcation nodes) in the channel network may also have a disproportionate effect on downstream flow routing and modelled patterns of flood inundation extent (Figure 6). Small changes in absolute bed elevation (relative to the total depth of the channel) at the Karnali bifurcation appear to drive changes in flow distribution into the two downstream branches (Figure 7). This is likely to occur through changes in channel gradient, where small amounts of sediment deposition or erosion may alter the gradient advantage down one branch (e.g. Kleinhans *et al.*, 2013). If the branches differ in depth, the amount of water and sediment entering – and the sediment transport capacity of each branch – are also expected to vary.

Historically, the dominant branch (i.e. carrying the greatest proportion of flow) downstream of the Karnali bifurcation is known to have switched numerous times. While the majority of flow is currently diverted down the west branch, switching of the dominant channel is thought to occur following large floods (Khanal *et al.*, 2016). The last shift in dominant channel from the east to the west branch occurred in 2010 following a large monsoonal flood discharge which had adverse effects on local Ganges river dolphin populations that were forced to relocate into the deeper but more heavily fished western branch (Paudel *et al.*, 2015; Khanal *et al.*, 2016). Landsat satellite imagery captured in November 2001 suggests that the dominant branch was also the west channel at this time, although in a slightly different location to the October 2016 branch (Figure 8). This implies that over the last ~18 years, there have been at least two changes in the dominant channel. Figure 8 suggests that changes in bed elevation at the Karnali river bifurcation, due to deposition and aggradation, lead to a switch in the dominant river channel, during both low- and peak-flow seasons. As the dominant channel changes, existing flood inundation models will have significantly reduced value, as they will

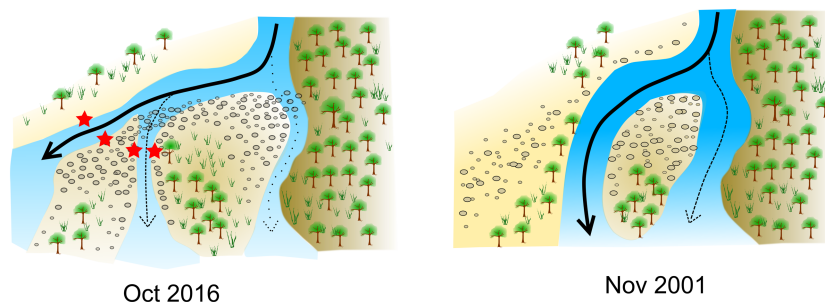


FIGURE 8. Schematic of Karnali river bifurcation. These images illustrate how the position of the bifurcation has migrated between 2016 and 2001 based on Landsat optical satellite imagery, where both schematics cover identical spatial frames. Solid lines represent the pathway of the main channel conveying the majority of flow, whilst dotted arrows represent secondary channels under low-flow conditions. Red stars shown in the October 2016 image correspond to the bank elevations shown in Figure 5a. [Colour figure can be viewed at wileyonlinelibrary.com]

likely underestimate inundation extent in the region surrounding the new dominant channel and overestimate it in the area where the dominant channel was originally located (Figure 6c). In general, the most mobile parts of the river system are situated downstream of the gravel–sand transition, where rates of lateral channel migration may be several hundred metres over a single year (Dingle *et al.*, 2020). Given the relative homogeneity of the floodplain, lateral shifting of the channel is likely just to extend the region of inundation in the direction of channel movement. If flow is routed into paleo-channels, these depressions across the landscape may route water further away into regions that were previously unaffected.

In river systems as dynamic as the Karnali, there is a need to constantly update and verify boundary conditions such as channel geometry and the channel boundary positions in order to improve predictive flood inundation models. Simply increasing DEM resolution does not necessarily improve model results dramatically. Capturing the dynamic nature of the fluvial network is especially important in low-relief aggrading landscapes that are often characterized by channels with high rates of lateral migration and avulsion. This can be achieved by resurveying the bathymetry and bank elevations following periods of sustained high water and sediment discharges or following channel avulsions. Surveys should be targeted at sensitive points in the landscape, such as the Karnali river bifurcation node, where changes in elevation have the greatest impact on downstream flow routing. Our inundation modelling demonstrates that ~2 m of vertical elevation change can change flood inundation extents by up to ~36%; improving the vertical accuracy of DEMs used in these types of predictive hydrodynamic modelling is key. Ensuring that DEMs are corrected for unrealistic channel depths is also necessary to produce more reliable flood prediction models and flood maps. Our results highlight the need to better understand and represent the physical processes that drive channel switching at topographically sensitive regions of channel networks (e.g. major channel bifurcation points) in such models. For example, how does switching of the dominant channel relate to the ability of a flow to mobilize bed material at these locations (i.e. threshold driven)? Or, is the frequency of channel switching also controlled by factors such as changes in sediment supply or sediment grain size?

The next stage of this work will be to develop these models to incorporate dynamic geomorphological processes (e.g. channel avulsion, bed aggradation and degradation, lateral migration) that dominate the dynamics of alluvial river systems downstream of many mountain ranges, not just the Himalaya (e.g. Constantine *et al.*, 2014; Martín-Vide *et al.*, 2014; Dingle *et al.*, 2019). Additional field data will be required to calibrate and validate these more complex flood models, including records of the extent of major flood events and collecting flow discharge, sediment concentration, and river cross-section measurements before, during, and after the monsoon season.

Conclusions

A field-calibrated 2D hydrodynamic flood model (Delft3D) of the Karnali River in west Nepal is presented. Flood inundation extents predicted for a 20-year flood are compared against outputs from an existing 1D HEC-RAS model using both the original 30m SRTM DEM (captured in 2000) and a new higher-resolution (10m) TanDEM-X DEM, captured in 2013, which more accurately reflects the current channel configuration. A number of scenarios were tested examining changing DEM resolution, variable bed elevation to simulate bed aggradation and incision, and updating bed elevations at a large

bifurcation node to reflect field observations. Modest quantities of bed aggradation or incision (relative to the bankfull depth of the channel) were found to significantly modify flood inundation extents across the low-relief landscape. Updating bed elevation at a major bifurcation node, based on field observations, resulted in switching of the dominant channel, reproducing observed flow distribution between the two river branches. This change in bed elevation across a small area of the bed resulted in an overall decrease in total inundation extent, but produced inundation of regions previously unaffected by the same flood discharge. Our results suggest that hydrodynamic models of mobile river systems need to be updated with field surveys of channel bathymetry and floodplain topography. Regular field measurements of bed elevation and updated DEMs following large sediment-generating events and at topographically sensitive areas, such as large river bifurcations, could help to improve model inputs in future flood prediction models. This is particularly important following large flood events carrying large sediment loads out of mountainous regions, which could lead to bed aggradation and channel switching in alluvial river systems further downstream. A fully integrated morphodynamic model of the Karnali River should be a goal for future studies, as and when high-quality fluvial field data become available.

Acknowledgements—This research was funded through a NERC Global Challenges Research Fund Building Resilience grant to H.D.S. (NE/P015905/1) and an EPSRC Global Challenges Research Fund Institutional Sponsorship grant (EP/P510944/1) to M.A. German Aerospace Center (DLR) project *gourmele_XTI_GLAC0296* provided the TanDEM-X data. The RTK-GPS was loaned from the NERC Geophysical Equipment Facility (loan 1088). We also thank Practical Action Consulting, Laura Quick, Bhairab Sitaula, and Nirajan Rayamajhee for assistance in the field and the Nepalese Department of Hydrology and Meteorology for the provision of discharge data. Finally, we thank Rajiv Sinha and two anonymous reviewers for comments that have improved the manuscript.

Data Availability Statement

The data that support the findings of this study are available from the corresponding author upon reasonable request.

Conflict of Interest

The authors declare no conflict of interest.

References

- Aalto R, Maurice-Bourgoin L, Dunne T, Montgomery DR, Nittrouer CA, Guyot JL. 2003. Episodic sediment accumulation on Amazonian floodplains influenced by El Niño/Southern Oscillation. *Nature* **425** (6957): 493–497.
- Carabajal CC, Harding DJ. 2006. SRTM C-band and ICESat laser altimetry elevation comparisons as a function of tree cover and relief. *Photogrammetric Engineering & Remote Sensing* **72**(3): 287–298.
- Chakraborty T, Kar R, Ghosh P, Basu S. 2010. Kosi megafan: historical records, geomorphology and the recent avulsion of the Kosi River. *Quaternary International* **227**(2): 143–160.
- Chen H, Petley DN. 2005. The impact of landslides and debris flows triggered by Typhoon Mindulle in Taiwan. *Quarterly Journal of Engineering Geology and Hydrogeology* **38**(3): 301–304.
- Coleman JM. 1969. Brahmaputra River: channel processes and sedimentation. *Sedimentary Geology* **3**(2–3): 129–239.
- Constantine JA, Dunne T, Ahmed J, Legleiter C, Lazarus ED. 2014. Sediment supply as a driver of river meandering and floodplain evolution in the Amazon Basin. *Nature Geoscience* **7**(12): 899–903.

- Dehecq A, Millan R, Berthier E, Gourmelen N, Trouvé E, Vionnet V. 2016. Elevation changes inferred from TanDEM-X data over the Mont-Blanc area: impact of the X-band interferometric bias. *IEEE Journal of Selected Topics in Applied Earth Observations and Remote Sensing* **9**(8): 3870–3882.
- Dingle EH, Sinclair HD, Attal M, Milodowski DT, Singh V. 2016. Subsidence control on river morphology and grain size in the Ganga Plain. *American Journal of Science* **316**(8): 778–812.
- Dingle EH, Attal M, Sinclair HD. 2017. Abrasion-set limits on Himalayan gravel flux. *Nature* **544**(7651): 471–474.
- Dingle EH, Paringit EC, Tolentino PL, Williams RD, Hoey TB, Barrett B, Long H, Smiley C, Stott E. 2019. Decadal-scale morphological adjustment of a lowland tropical river. *Geomorphology* **333**: 30–42.
- Dingle EH, Sinclair HD, Venditti J, Attal M, Kinnaird TC, Creed M, Quick L, Nittrouer JA, Gautam D. 2020. Sediment dynamics across gravel–sand transitions: implications for river stability and floodplain recycling. *Geology* **48**: 468–472.
- Eineder M, Jaber WA, Floricioiu D, Rott H, Yague-Martinez N. 2011. Glacier flow and topography measurements with TerraSar-X and TanDEM-X. In *2011 IEEE International Geoscience and Remote Sensing Symposium*; 3835–3838.
- Flemings PB, Jordan TE. 1989. A synthetic stratigraphic model of foreland basin development. *Journal of Geophysical Research - Solid Earth* **94**(B4): 3851–3866.
- Goswami DC. 1985. Brahmaputra River, Assam, India: physiography, basin denudation, and channel aggradation. *Water Resources Research* **21**(7): 959–978.
- Grieve SW, Mudd SM, Milodowski DT, Clubb FJ, Furbish DJ. 2016. How does grid-resolution modulate the topographic expression of geomorphic processes? *Earth Surface Dynamics* **4**(3): 627–653.
- Keefer DK. 1999. Earthquake-induced landslides and their effects on alluvial fans. *Journal of Sedimentary Research* **69**(1): 84–104.
- Khanal G, Suryawanshi KR, Awasthi KD, Dhakal M, Subedi N, Nath D, Kandel RC, Kelkar N. 2016. Irrigation demands aggravate fishing threats to river dolphins in Nepal. *Biological Conservation* **204**: 386–393.
- Kleinhans MG, Ferguson RI, Lane SN, Hardy RJ. 2013. Splitting rivers at their seams: bifurcations and avulsion. *Earth Surface Processes and Landforms* **38**(1): 47–61.
- Krieger G, Moreira A, Fiedler H, Hajnsek I, Werner M, Younis M, Zink M. 2007. TanDEM-X: a satellite formation for high-resolution SAR interferometry. *IEEE Transactions on Geoscience and Remote Sensing* **45**(11): 3317–3341.
- Lane SN, Tayefi V, Reid SC, Yu D, Hardy RJ. 2007. Interactions between sediment delivery, channel change, climate change and flood risk in a temperate upland environment. *Earth Surface Processes and Landforms: The Journal of the British Geomorphological Research Group* **32**(3): 429–446.
- Lupker M, Blard PH, Lavé J, France-Lanord C, Leanni L, Puchol N, Charreau J, Bourlès D. 2012. ¹⁰Be-derived Himalayan denudation rates and sediment budgets in the Ganga basin. *Earth and Planetary Science Letters* **333**: 146–156.
- Martín-Vide JP, Amarilla M, Zárate FJ. 2014. Collapse of the Pilcomayo River. *Geomorphology* **205**: 155–163.
- Montgomery DR, Panfil MS, Hayes SK. 1999. Channel-bed mobility response to extreme sediment loading at Mount Pinatubo. *Geology* **27**(3): 271–274.
- Parsons DR, Jackson PR, Czuba JA, Engel FL, Rhoads BL, Oberg KA, Best JL, Mueller DS, Johnson KK, Riley JD. 2013. Velocity Mapping Toolbox (VMT): a processing and visualization suite for moving-vessel ADCP measurements. *Earth Surface Processes and Landforms* **38**: 1244–1260.
- Paudel S, Timilsina YP, Lewis J, Ingersoll T, Jnawali SR. 2015. Population status and habitat occupancy of endangered river dolphins in the Karnali river system of Nepal during low water season. *Marine Mammal Science* **31**(2): 707–719.
- Pelletier JD. 2013. A robust, two-parameter method for the extraction of drainage networks from high-resolution digital elevation models (DEMs): evaluation using synthetic and real-world DEMs. *Water Resources Research* **49**(1): 75–89.
- Quick L, Sinclair HD, Attal M, Singh V. 2019. Conglomerate recycling in the Himalayan foreland basin: implications for grain size and provenance. *Geological Society of America Bulletin* **132**(7–8): 1639–1656. <https://doi.org/10.1130/B35334.1>
- Rana N, Singh S, Sundriyal YP, Juyal N. 2013. Recent and past floods in the Alaknanda valley: causes and consequences. *Current Science* **105**(9): 1209–1212.
- Risk Nexus. 2015. *Urgent case for recovery: what we can learn from the August 2014 Karnali River floods in Nepal*. Written by Institute for Social and Environmental Transition (ISET International and ISET-Nepal), Practical Action Nepal and the Zurich Insurance Company.
- Rodriguez E, Morris CS, Belz JE. 2006. A global assessment of the SRTM performance. *Photogrammetric Engineering & Remote Sensing* **72**(3): 249–260.
- Sinha R. 2009. The great avulsion of Kosi on 18 August 2008. *Current Science* **97**(3): 429–433.
- Sinha R, Friend PF. 1994. River systems and their sediment flux, Indo-Gangetic plains, Northern Bihar, India. *Sedimentology* **41**(4): 825–845.
- Sinha R, Jain V, Babu GP, Ghosh S. 2005. Geomorphic characterization and diversity of the fluvial systems of the Gangetic Plains. *Geomorphology* **70**(3–4): 207–225.
- Slater LJ, Singer MB, Kirchner JW. 2015. Hydrologic versus geomorphic drivers of trends in flood hazard. *Geophysical Research Letters* **42**(2): 370–376.
- Slater LJ, Khouakhi A, Wilby RL. 2019. River channel conveyance capacity adjusts to modes of climate variability. *Scientific Reports* **9**(1): 1–10.
- Stover S, Montgomery DR. 2001. Channel change and flooding, Skokomish River, Washington. *Journal of Hydrology* **234**(3–4): 272–282.
- Tandon SK, Gibling MR, Sinha R, Singh V, Ghazanfari P, Dasgupta A, Jain M, Jain V. 2006. *Alluvial Valleys of the Ganga Plains, India: Timing and Causes of Incision*. SEPM: Paris.
- Wendi D, Liong SY, Sun Y, Doan CD. 2016. An innovative approach to improve SRTM DEM using multispectral imagery and artificial neural network. *Journal of Advances in Modeling Earth Systems* **8**(2): 691–702.
- Wessel B, Huber M, Wohlfart C, Marschalk U, Kosmann D, Roth A. 2018. Accuracy assessment of the global TanDEM-X Digital Elevation Model with GPS data. *ISPRS Journal of Photogrammetry and Remote Sensing* **139**: 171–182.

Supporting Information

Additional supporting information may be found online in the Supporting Information section at the end of the article.

Table S1. Changes in inundation extent for water depths greater than 0.05 m for different model configurations and scenarios.

Figure S1. Estimated return interval for annual peak discharge measurements from 1962 to 2014 at Chisapani gauging station (black dots). Projected return interval estimated using a Gumbel distribution (grey line) and upper and lower 95% confidence limits (blue and red dot-dashed lines, respectively).

Figure S2. Discharge hydrograph used as model input. Discharge measurements recorded by DHM at Chisapani gauging station from 1 February to 30 July 2013.

Figure S3. Inundation extent and water depth (>0.05 m) for a 1 in 20-year flood discharge for (a) the existing HEC-RAS hydrodynamic model and SRTM DEM, (b) using the new Delft3D model and SRTM DEM, (c) for Scenario 1 using the Delft3D model and new 10 m TanDEM-X DEM, and (d) for Scenario 1 using the Delft3D model and 30 m resampled TanDEM-X DEM